Adult mouse epicardium modulates myocardial injury by secreting paracrine factors

Bin Zhou,[1,2,3] Leah B. Honor,[1,2] Huamei He,[4] Qing Ma,[1,2] Jin-Hee Oh,[1,5] Catherine Butterfield,[6] Ruei-Zeng Lin,[7] Juan M. Melero-Martin,[7] Elena Dolmatova,[8] Heather S. Duffy,[8] Alexander von Gise,[1,2] Pingzhu Zhou,[1,2] Yong Wu Hu,[1,2] Gang Wang,[1,2] Bing Zhang,[1,2] Lianchun Wang,[9] Jennifer L. Hall,[10] Marsha A. Moses,[9] Francis X. McGowan,[4] and William T. Pu[1,2]

[1]Department of Cardiology, Children's Hospital Boston, Boston, Massachusetts, USA. [2]Harvard Stem Cell Institute, Harvard University, Cambridge, Massachusetts, USA. [3]Institute for Nutritional Sciences, Shanghai Institutes for Biological Sciences, Chinese Academy of Sciences, Shanghai, China. [4]Department of Anesthesiology, Perioperative, and Pain Medicine, Children's Hospital Boston, Boston, Massachusetts, USA. [5]Department of Pediatrics, Catholic University of Korea, Seoul, South Korea. [6]Vascular Biology Program, Children's Hospital Boston, and Department of Surgery, Harvard Medical School, Boston, Massachusetts, USA. [7]Department of Cardiac Surgery, Children's Hospital Boston, and Department of Surgery, Harvard Medical School, Boston, Massachusetts, USA. [8]Cardiovascular Medicine, Beth Israel Deaconess Medical Center, Boston, Massachusetts, USA. [9]Complex Carbohydrate Research Center, Department of Biochemistry and Molecular Biology, University of Georgia, Athens, Georgia, USA. [10]Lillehei Heart Institute, University of Minnesota, Minneapolis, Minnesota, USA.

The epicardium makes essential cellular and paracrine contributions to the growth of the fetal myocardium and the formation of the coronary vasculature. However, whether the epicardium has similar roles postnatally in the normal and injured heart remains enigmatic. Here, we have investigated this question using genetic fate-mapping approaches in mice. In uninjured postnatal heart, epicardial cells were quiescent. Myocardial infarction increased epicardial cell proliferation and stimulated formation of epicardium-derived cells (EPDCs), which remained in a thickened layer on the surface of the heart. EPDCs did not adopt cardiomyocyte or coronary EC fates, but rather differentiated into mesenchymal cells expressing fibroblast and smooth muscle cell markers. In vitro and in vivo assays demonstrated that EPDCs secreted paracrine factors that strongly promoted angiogenesis. In a myocardial infarction model, EPDC-conditioned medium reduced infarct size and improved heart function. Our findings indicate that epicardium modulates the cardiac injury response by conditioning the subepicardial environment, potentially offering a new therapeutic strategy for cardiac protection.

Introduction

Myocardial infarction (MI) causes cardiomyocyte loss that far exceeds the limited regenerative capacity of mammalian myocardium (1), resulting in substantial morbidity and mortality. Progress in developing new therapies hinges on understanding the myocardial injury response elicited by MI. Recent studies in zebrafish, a vertebrate model capable of heart regeneration, suggested that the epithelial cell sheet covering the heart, the epicardium, plays a pivotal role in its regenerative response (2). In mammals, the fetal epicardium secretes factors that promote growth of myocardium. Epicardium also makes essential cellular contributions to the fetal myocardium, undergoing epithelial-to-mesenchymal transition (EMT) to form epicardium-derived cells (EPDCs) that differentiate into cardiomyocyte, coronary EC, smooth muscle cell, and interstitial fibroblast lineages (3–7). These data raise the tantalizing possibility that adult mammalian epicardium might be recruited for use in therapeutic myocardial regeneration. However, little is known about the roles of epicardium in the adult mammalian heart, either in organ homeostasis or in response to myocardial injury. Improved understanding of the pathophysiology of the myocardial injury response is fundamental for development of novel regenerative approaches for heart disease.

A major block to gaining greater insight into the function of adult epicardium has been an inability to specifically trace these cells in vivo and to isolate a pure population of EPDCs for fur-

ther characterization and analysis in vitro. Here, we overcame this hurdle using 2 independent Cre-loxP–based approaches to specifically label epicardium and its derivatives. We tested the hypothesis that adult epicardium differentiates into other myocardial lineages in the adult heart. Furthermore, we isolated and characterized genetically marked EPDCs, permitting further analysis of their function using in vitro and in vivo models. Our results indicated that epicardial cells were activated by myocardial injury and formed an expanded layer of EPDCs. These EPDCs remained mesenchymal and did not adopt cardiomyocyte or coronary EC fates. However, they engaged in the myocardial injury response, promoting coronary vessel growth by conditioning the subepicardial region through paracrine mechanisms. Remarkably, injection of EPDC-conditioned media (EPDC-CM) in a MI model reduced infarct size and improved cardiac function. These results suggest that augmentation of properties of native epicardium may be an attractive therapeutic strategy in cardiac repair and regeneration.

Results

Epicardial cells do not undergo EMT in normal adult heart. We used inducible Cre-loxP technology to selectively and irreversibly label adult epicardial cells and their derivatives. CreERT2, a tamoxifen-activated (tam-activated) fusion of Cre recombinase to an engineered hormone binding domain of the estrogen receptor (ESR1), was selectively expressed in epicardium by knocking it into the *Wt1* locus (*Wt1^{CreERT2}*) (4). In fetal heart, cardiac WT1 expression was largely restricted to the epicardium (refs. 4, 5, Figure 1A, and
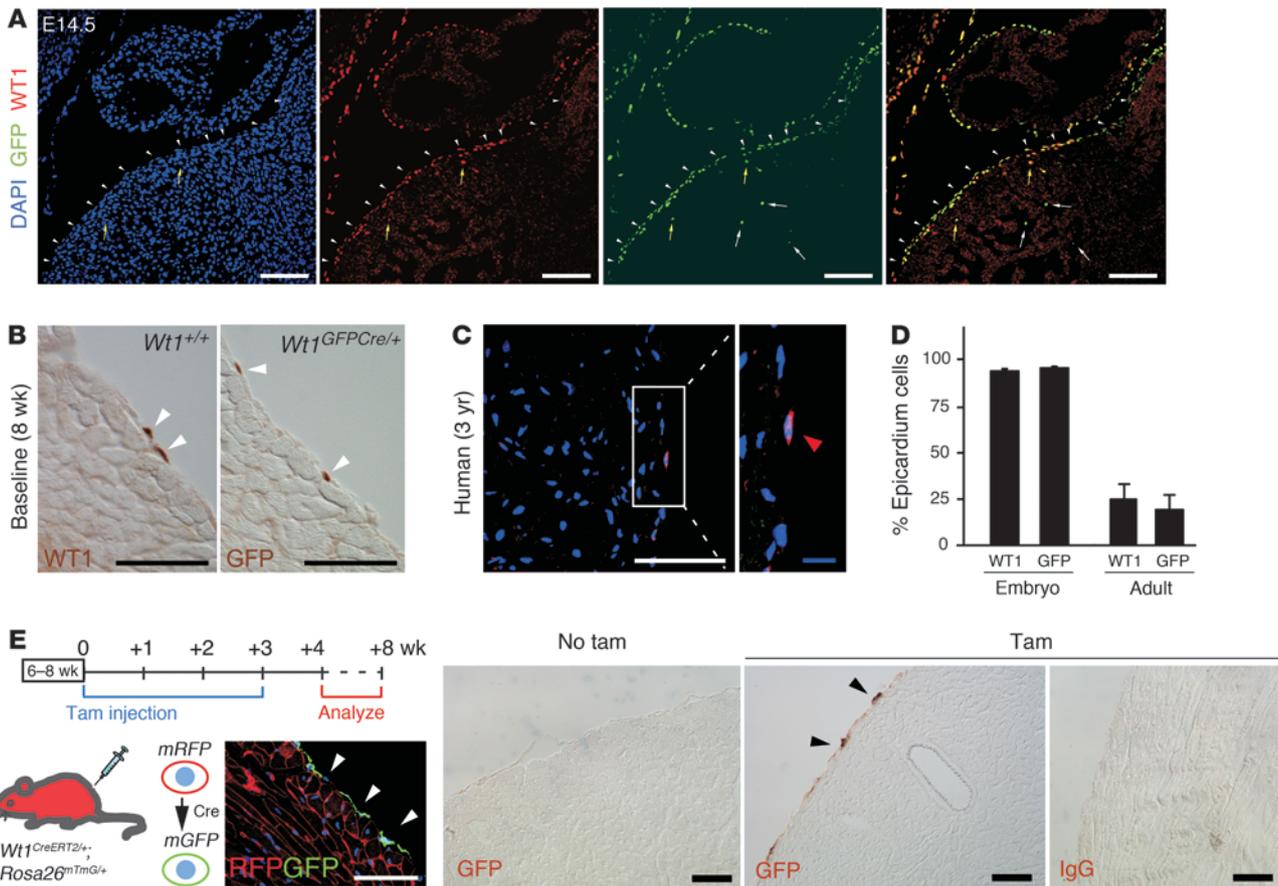
Figure 1
Epicardium is quiescent in the normal postnatal heart. (**A**) Expression of WT1 and *Wt1*-driven fusion protein epitope GFP (*Wt1*$^{GFPCre/+}$) in fetal epicardium. White arrowheads, epicardial expression of GFP and WT1; yellow arrows, subepicardial migrating EPDC still expressing WT1 and GFP; white arrows, blood cells inside myocardium. (**B**) Expression of WT1 or GFP (white arrowheads) in postnatal epicardium. (**C**) WT1 was also expressed in postnatal human epicardium (red arrowhead). (**D**) Quantitation of WT1$^+$ or GFP$^+$ epicardial cells in *Wt1*$^{GFPCre/+}$ hearts (*n* = 3–6). (**E**) Experimental outline for genetic fate mapping in normal postnatal heart using *Wt1*$^{CreERT2/+}$;*Rosa26*$^{mTmG/+}$ mice. Tam irreversibly changed expression of membrane-localized RFP to membrane-localized GFP (arrowheads). In normal mice, Cre activity was strictly tam dependent. Scale bars: 100 μm; 20 μm (**C**, right).

Supplemental Figure 1; supplemental material available online with this article; doi:10.1172/JCI45529DS1). In postnatal mouse and human heart, WT1 was also detected in epicardial cells (Figure 1, B and C), although at a reduced frequency compared with fetal epicardium (Figure 1D). Activation of Cre by tam treatment of uninjured adult *Wt1*$^{CreERT2/+}$ mice allowed us to track the fate of adult epicardial cells during heart homeostasis. Epicardial cells with a history of Cre activity were identified using the reporter *Rosa26*$^{mTmG/+}$, which heritably switched from RFP to GFP expression upon Cre recombination (Figure 1E). We did not detect GFP in the absence of tam (Figure 1E and Supplemental Figure 4A), which is indicative of tight control of Cre activity in this system. From 1 to 8 weeks after tam treatment, a subset of epicardial cells expressed GFP (Figure 1E). These cells resided on the surface of the heart, did not migrate into myocardium, and did not express cardiomyocyte, endothelial, or smooth muscle cell markers (data not shown). We did detect rare GFP$^+$ cells within the myocardium that expressed EC markers (Supplemental Figure 2, A–E), but these were likely caused by endogenous expression of Wt1 in rare ECs (Supplemental Figure 2, F–H) rather than by differentiation of epicardial cells into ECs.

The lack of cells within uninjured myocardium lineage-marked by *Wt1*^{CreERT2} might reflect technical limitations of this approach. Therefore, we used an independent lineage-tracing method based on injection of Ad:Msln-Cre, an adenovirus in which the epicardially restricted mesothelin (*Msln*) promoter (8, 9) drives Cre expression. MSLN was expressed in adult epicardium and cultured epicardial cells, and cardiac expression remained confined to epicardium after MI (Supplemental Figure 3A and data not shown). Ultrasound-guided delivery of Ad:Msln-Cre to *Rosa26*$^{mTmG/+}$ heart specifically labeled epicardium (Supplemental Figure 3, B and C). At 4 weeks after virus injection, nearly all Cre-dependent GFP lineage tracer was on the surface of the heart (Supplemental Figure 3, D and E), in WT1$^+$ and RALDH2$^+$ epicardial cells. We did not detect any GFP$^+$ cells that expressed EC markers in this model (Supplemental Figure 3F).

Response of epicardium to heart injury. We investigated the participation of epicardium in the cardiac injury response. Fetal epicardial genes *Wt1*, *Tbx18*, and *Raldh2* were dynamically upregulated after MI, peaking between 1 and 5 days and declining to near-baseline levels by 4 weeks (Figure 2A). Organ-wide, the epicardial region increased to several cells thick. The thickening was most pro-
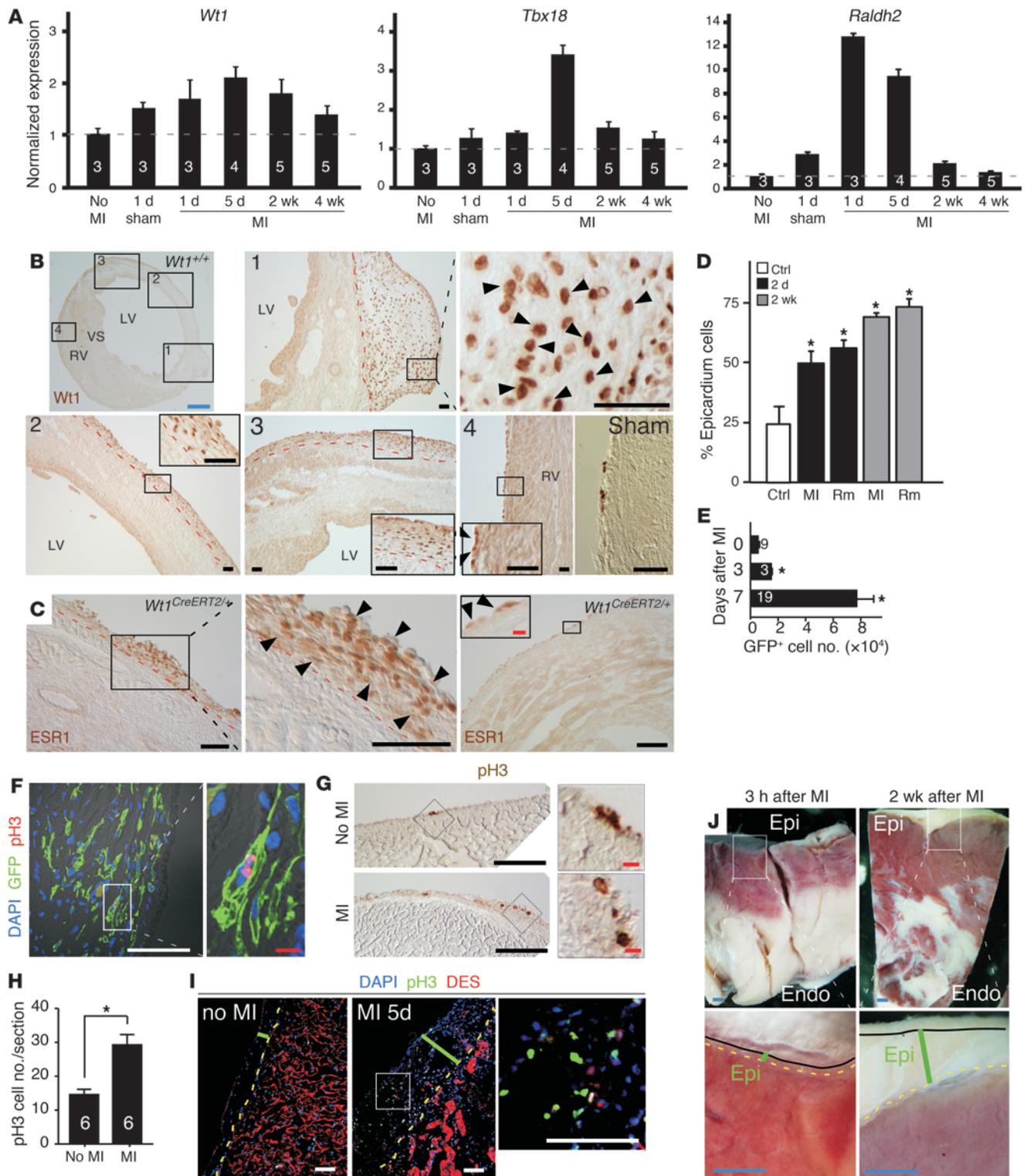
Figure 2

Reactivation of the fetal epicardial program after MI. (**A**) qRT-PCR of heart RNA for epicardial genes after MI or sham operation, expressed relative to normal heart (no MI). (**B**) Immunohistochemistry of WT1 in heart 2 weeks after MI or sham operation. Epicardial thickening and WT1 upregulation were observed overlying infarct (regions 1 and 2), peri-infarct (region 3), and remote myocardium (region 4). Arrowheads indicate WT1 expression. (**C**) Expansion of the Wt1-expressing epicardial region at border zone and remote areas, confirmed by immunostaining for the CreERT2 epitope ESR1 in $Wt1^{CreERT2/+}$ heart cryosections 2 weeks after MI. Arrowheads, ESR1$^+$ cells in the epicardial region. (**D**) Quantitation of WT1$^+$ epicardial cells after MI. Epicardium overlying remote (Rm) and infarct (MI) myocardium is shown. $n = 3–6$. (**E**) Number of GFP$^+$ cells in adult labeled $Wt1^{CreERT2/+}$; $Rosa26^{mTmG/+}$ hearts after MI, as measured by FACS. (**F**) Proliferation of GFP-labeled EPDC after MI, detected by pH3 staining. (**G** and **H**) Epicardial proliferation increased, as assessed by pH3 staining, 3 days to 2 weeks after MI. Shown are (**G**) representative images and (**H**) quantification. (**I**) pH3 staining on canine myocardium. Canine epicardial cells increased proliferation between no MI and 5 days after MI. (**J**) Representative wedges of dog heart showing epicardium thickness 3 hours and 2 weeks after MI. Black line, outer layer of epicardium; green bar, epicardial thickness; dashed yellow and red lines, border between epicardium and myocardium. Scale bars: 100 μm; 1 mm (**B**, top left, and **J**); 10 μm (**C**, inset; **F** and **G**, right). n is shown for each group in **A**, **E**, and **H**. *$P < 0.05$ versus control.

nounced in the vicinity of the infarct (Figure 2B). We investigated in detail the expression map of WT1 in infarcted heart to facilitate interpretation of epicardial lineage tracing using the $Wt1^{CreERT2/+}$ allele. WT1 was upregulated in a region overlying the myocardium containing epicardium and its derivatives (Figure 2B), so that the fraction of WT1$^+$ cells increased from approximately 25% in normal heart to approximately 75% after MI (Figure 2D). We independently confirmed expansion of this population by staining for the ESR1 epitope of the CreERT2 fusion protein in $Wt1^{CreERT2/+}$ hearts (Figure 2C) and by fluorescence-activated cell sorting (FACS) analysis, which showed a 12-fold increase of $Wt1^{CreERT2}$-labeled cells after MI (normal, 6.3×10^3 cells/heart; after MI, 78.1×10^3 cells/heart; Figure 2E). Pericardial opening was insufficient to stimulate Wt1 upregulation and epicardial expansion, as neither was observed with sham operation (Figure 2B). Consistent with expansion of $Wt1$-derived epicardial cells after MI, phospho-histone H3 (pH3) and BrdU staining showed that $Wt1^{CreERT2}$-marked cells in the epicardial region were highly proliferative 2 days after MI (Figure 2, F–H, and data not shown). To determine whether proliferation and expansion of the epicardial region occurs in larger mammals, we also examined canine myocardium obtained at baseline and between 5 days and 2 weeks after MI. As in the mice, MI induced cells in the canine epicardial region to become highly proliferative, and the epicardial region substantially increased in thickness in canine-infarcted heart (Figure 2, I and J). These data indicate that MI reactivates a fetal program, including increased proliferation and upregulation of fetal genes.

A hallmark of fetal epicardium is the formation of mesenchymal cells by EMT. Due to the lack of lineage-tracing tools, there has been a paucity of direct in vivo evidence to evaluate whether this process occurs in adult heart injury. Here we used our genetic mouse models to directly track the fate of epicardial cells in infarcted heart and to isolate pure populations of post-MI EPDCs for further analysis. In the normal adult heart, epicardial EMT appeared quiescent (Figure 1). We asked whether it was reactivated by myocardial injury. To

selectively label epicardial cells and their derivatives with GFP and track their fate after MI, we treated adult $Wt1^{CreERT2/+}$;$Rosa26^{mTmG/+}$ mice with tam, then induced MI by coronary artery ligation (Figure 3A). In tam-treated MI hearts, 24.6% ± 2.5% of epicardial cells were GFP$^+$, which indicated labeling of a substantial fraction of cells. Control experiments established the specificity of this labeling protocol (Supplemental Figure 4, A–H). In mice not treated with tam and subjected to MI, we detected very rare GFP$^+$ cells (0.6% ± 0.5% of epicardial cells) that were confined to the epicardial layer. Because these cells were rare and limited to the epicardial layer, this "leaky" Cre activity induced by MI stress did not impair interpretation of subsequent experiments.

The GFP$^+$ cells, composed of epicardium and its derivatives, are hereafter collectively referred to as EPDCs. To evaluate whether EPDCs arise from adult Wt1$^+$ epicardial cells through EMT, we used FACS to isolate cells highly enriched for EPDCs. Validation studies showed that the FACS-purified EPDCs were highly enriched for epicardial markers and depleted for myocardial markers (Supplemental Figure 5A). We next measured expression of EMT-related genes in FACS-purified EPDCs. Compared with non-EPDCs, EPDCs were enriched for $Snail$, $Slug$, $Twist$, and $Smad1$ (Supplemental Figure 5B). Cardiac expression of these transcripts changed dynamically following MI, with maximal expression observed 5 days after MI (Supplemental Figure 5C). Immunostaining of infarcted mouse heart for EMT-regulatory proteins further confirmed this result, demonstrating upregulation of pSMAD1/5/8, pSMAD2, SNAIL, and SLUG in the epicardial region (Supplemental Figure 5, D–G). Consistent with their origin via EMT, FACS-sorted EPDCs had a mesenchymal rather than epithelial morphology (Supplemental Figure 5H). Collectively, these data support reactivation of epicardial EMT after MI.

EPDC fate after MI. We used genetic lineage tracing to examine the fate of EPDCs after MI (Figure 3A). GFP-marked EPDCs remained in the epicardial region overlying the heart and did not migrate into myocardium (Figure 3, B–F). In 24 MI hearts, after excluding autofluorescence signals by spectral analysis (Supplemental Figure 6, A–G), we did not detect EPDCs that coexpressed cardiomyocyte markers TNNT2 or ACTN2 (Figure 3, C and D), which indicates that EPDCs do not give rise to cardiomyocytes in the adult mouse heart after MI. Similarly, within the thickened epicardial region, we did not detect EPDCs that coexpressed endothelial markers (Figure 3E). We did find rare GFP$^+$ cells within the myocardium, and all of these rare cells expressed endothelial markers (Figure 3F). GFP labeling of these cells was likely due to $Wt1$-driven CreERT2 expression in some coronary ECs (10), rather than EPDCs that had migrated into the myocardium (Supplemental Figure 6, H–K), as there was no spatial relationship of these cells to the epicardium even shortly after MI. We conclude that EPDCs did not adopt cardiomyocyte or EC fates after MI.

In fetal heart, EPDCs largely differentiate into smooth muscle and fibroblast lineages (5–7). In adult heart after MI, EPDCs also expressed fibroblast-specific protein 1 (FSP1), procollagen I (ProCol), collagen III (ColIII), fibronectin (FN1), α-SMA, SM22α, and smooth muscle myosin heavy chain (SM-MHC), markers of mesenchymal lineages including fibroblasts, myofibroblasts, and smooth muscle cells (Figure 3, G–M). Differentiation of EPDCs into these mesenchymal lineages was independently confirmed by analysis of FACS-purified EPDCs, which were highly enriched for markers of these lineages by immunostaining (Supplemental Figure 7, A–L) and by quantitative RT-PCR; Supplemental Figure 7M). FACS-purified EPDCs also
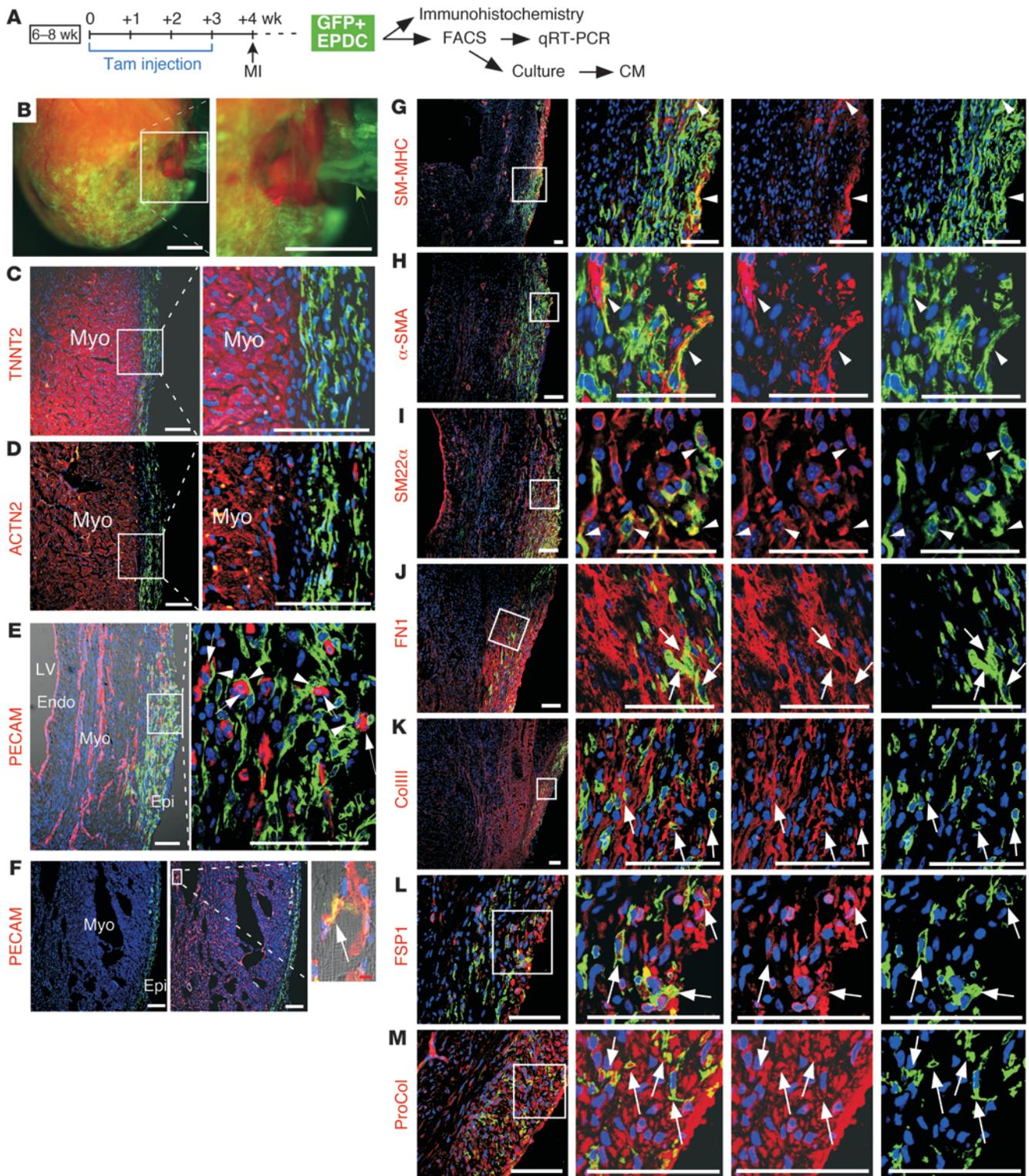
Figure 3
Fate of EPDCs after MI. EPDCs marked by GFP lineage tracer (green) were analyzed for coexpression of differentiation markers (red) after MI. Images are representative of 2 weeks after MI; similar results were observed at 1 week, 4 weeks, and 3 months. (**A**) EPDC labeling protocol. (**B**) Whole-mount image of *Wt1*$^{CreERT2/+}$*;Rosa26*$^{mTmG/+}$ heart after MI. GFP was present in the epicardial region (green arrow), whereas myocardium was mainly GFP$^-$ (red arrow). A region of epicardium was lifted off of the heart to improve visualization. (**C** and **D**) EPDCs did not express cardiomyocyte markers TNNT2 or ACTN2. (**E** and **F**) EPDCs (arrowheads, **E**) did not express endothelial marker PECAM in the epicardial region, but were frequently adjacent to ECs (arrows, **E**). Within the myocardium, very rare GFP$^+$ cells were observed; these cells expressed PECAM (arrow, **F**). (**G**–**I**) A subset of EPDCs expressed smooth muscle markers SM-MHC (**G**), α-SMA (**H**), and SM22α (**I**). (**J**–**M**) A subset of EPDCs expressed mesenchymal/fibroblast markers FN1 (**J**), ColIII (**K**), FSP1 (**L**), and ProCol (**M**). Scale bars: 100 μm; 1 mm (**B**); 10 μm (**F**, right). Myo, myocardium; Endo, endocardium; Epi, epithelium.

lacked expression of cardiomyocyte markers ACTN2 and TNNT2 and of endothelial marker PECAM (Supplemental Figure 7, F–H). These data indicate that adult EPDCs differentiate into smooth muscle, myofibroblast, and fibroblast lineages after MI, but do not adopt a cardiomyocyte fate as previously described (11).

To confirm the above result, we used ultrasound-guided delivery of Ad:Msln-Cre to selectively label epicardium by an independent method. We injected Ad:Msln-Cre into adult *Rosa26*[mTmG/+] heart to label epicardial cells, induced experimental MI, and then analyzed hearts 3 days to 4 weeks after MI (Supplemental Figure 8A). Consistent with *Wt1*[CreERT2] labeling results, Ad:Msln-Cre–labeled epicardial cells were observed in the epicardial region covering the heart (Supplemental Figure 8, B–E). GFP+ cells within the epicardial region expressed the mesenchymal cell marker FSP1 and did not express endothelial or cardiomyocyte markers (Supplemental Figure 8, F and G). We also did not observe any GFP+ ECs within the myocardium, which again indicated that *Wt1*[CreERT2]-labeled GFP+ ECs observed in the post-MI heart are likely to arise from *Wt1*[CreERT2] expression in these cells. We concluded that after MI, epicardial cells undergo EMT and adopt mesenchymal cell fates. These mesenchymal cells remain in the epicardial region and differentiate primarily into fibroblast and smooth muscle cells, but do not reconstitute cardiomyocyte or coronary ECs.

EPDCs secrete growth factors and promote angiogenesis. Whereas EPDCs within the thickened epicardial region did not adopt EC fates, ECs were common in this area and were frequently located adjacent to EPDCs (Figure 3E). Similarly, ECs were frequently observed in the epicardial region in canine heart after MI (data not shown). These observations are reminiscent of the close relationship between epicardium and coronary vasculature during heart development (12, 13), where coronary vasculature first develops immediately below the epicardium. To directly test the proangiogenic role of the expanded epicardial region in adult post-MI heart, we FACS-purified EPDCs from infarcted hearts and expanded them in culture (Supplemental Figure 9). After amplification for 5 passages, EPDCs continued to exhibit mesenchymal morphology (Figure 4A) and retained their high purity (>99.5% GFP+, Supplemental Figure 9, C and D). Expression of selected surface markers were stable between initial culture (i.e., passage 0 [P0]) and P5 (Supplemental Figure 9E). Epicardial markers *Wt1* and *Tbx18* continued to be expressed at P5, although their levels decreased approximately 50% (Supplemental Figure 9F).

EPDC-CM from P5 EPDCs stimulated growth of multiple types of ECs — human cord blood ECs (cbECs), HUVECs, cardiac microvasculature ECs, immortalized lung ECs, and bovine capillary ECs — to a degree comparable to that stimulated by 5% FBS or media conditioned by mouse bone marrow mesenchymal stem cells (MSCs; Figure 4, B–D, Supplemental Figure 10, A–F, and data not shown), which have established angiogenic activity (14). EPDC-CM from 8 independent EPDC cultures significantly increased EC number, measured by both direct cell counting and MTT assays, and the growth-promoting effect was observed at up to 72 hours of incubation and 1:80 dilution (Figure 4, B–D, and Supplemental Figure 10, A–F). Boiling abolished the growth-promoting effect (Figure 4D), consistent with essential heat-labile factors such as proteins. EPDC-CM promoted growth by both reducing apoptosis (Figure 4E) and stimulating proliferation (EPDC-CM, 5.8% BrdU+ cells; control media, 1.4% BrdU+ cells, *P* < 0.05; Figure 4, E and F). Together, these data indicate that EPDC-secreted factors promote EC growth.

In addition to stimulating EC growth, EPDC secreted factors stimulated vessel assembly. When cocultured with ECs, EPDCs incorporated into the EC vessel network (Figure 4G and Supplemental Figure 11, A and B), suggestive of potential cellular contribution as pericytes or smooth muscle cells to promote vessel formation and maturation. This is consistent with the frequent position of EPDCs next to ECs in both mouse and dog heart after MI (Figure 3E and data not shown). To further study the effect of EPDCs on vessel assembly in an in vivo model, we used the Matrigel plug assay (Figure 4H). Whereas cbECs formed scant vessels in Matrigel plugs lacking EPDCs, they formed robust vessels in the presence of EPDCs, comparable to what was observed by the combination of cbECs with MSCs (Figure 4, I and J, and Supplemental Figure 11, C and D). EPDCs, marked by GFP, were located adjacent to human ECs, labeled with UEA, a lectin that specifically labels human ECs (Figure 4K). EPDCs expressed NG2, CNN, SM22, and SMA, markers of pericytes and smooth muscle cells (Figure 4, L and M, and Supplemental Figure 11, E and F). As we observed in heart tissue (Figure 3), EPDCs did not adopt an EC fate in this assay (Figure 4K and Supplemental Figure 11G). Blood vessels assembled in the Matrigel plugs formed functional connections to the host circulatory system, as tail vein injection of UEA labeled vessels within the plugs (Figure 4N). Moreover, Matrigel plugs containing only EPDCs without implanted ECs developed blood vessels (Supplemental Figure 11, H and I), which indicates that EPDCs alone stimulate host angiogenesis. Additionally, the cornea micropocket assay provided further in vivo evidence of angiogenic activity of EPDC-secreted factors. Corneal implantation of EPDC-CM–loaded pellets promoted vessel growth on the normally avascular cornea, whereas pellets loaded with unconditioned media did not (Supplemental Figure 11J). Together, these data show the proangiogenic activity of EPDC-secreted factors.

To identify molecules responsible for CM proangiogenic activity, we screened EPDCs for enriched expression of angiogenic factors by qRT-PCR. A large number of proangiogenic transcripts were highly enriched in EPDCs compared with non-EPDCs, including *Vegfa*, *Angpt1*, *Ang*, *Fgf1*, *Fgf2*, *Fgf9*, *Pdgfa*, *Pdgfc*, *Pdgfd*, *Adamts1*, *Sdf1*, *Mcp1*, and *Il6* (Figure 5A). These genes were also expressed in cultured EPDCs, and their expression was maintained between P0 and P5 (Supplemental Figure 10G). To investigate whether MI alters expression of these genes in *Wt1*[CreERT2] lineage cells, we compared the angiogenic gene expression profile of EPDCs after MI with the small subset of epicardial cells labeled by *Wt1*[CreERT2] in non-MI heart. Several angiogenic genes were either up- or downregulated, although there was no systematic change in the angiogenic profile (Supplemental Figure 12). These data suggest that amplification of EPDC number after MI is an important contributor to the epicardium's effects on angiogenesis. However, *Sdf1* and *Mcp1*, chemotactic factors for circulating cells active in angiogenesis, were highly upregulated by MI, which indicates that MI significantly alters expression of additional epicardial genes relevant to the myocardial injury response.

An angiogenesis antibody array confirmed post-MI EPDC secretion of VEGFA, SDF1, MCP1, IGFPBP2, IGFPBP3, IGFPBP9, and IGFPBP10 at the protein level (Figure 5B). Blocking antibodies to these factors indicated that FGF2 and VEGFA accounted for approximately half the growth-promoting activity of CM on ECs (Figure 5C). However, EPDC-CM treated with both FGF2 and VEGFA blocking antibodies retained some growth-stimulating activity (Figure 5C), suggestive of additional factors or combined effects of multiple factors. Consistent with these cell culture data, we observed strong expression of VEGFA and FGF2 in the epicardial region of the post-MI heart (data not shown).
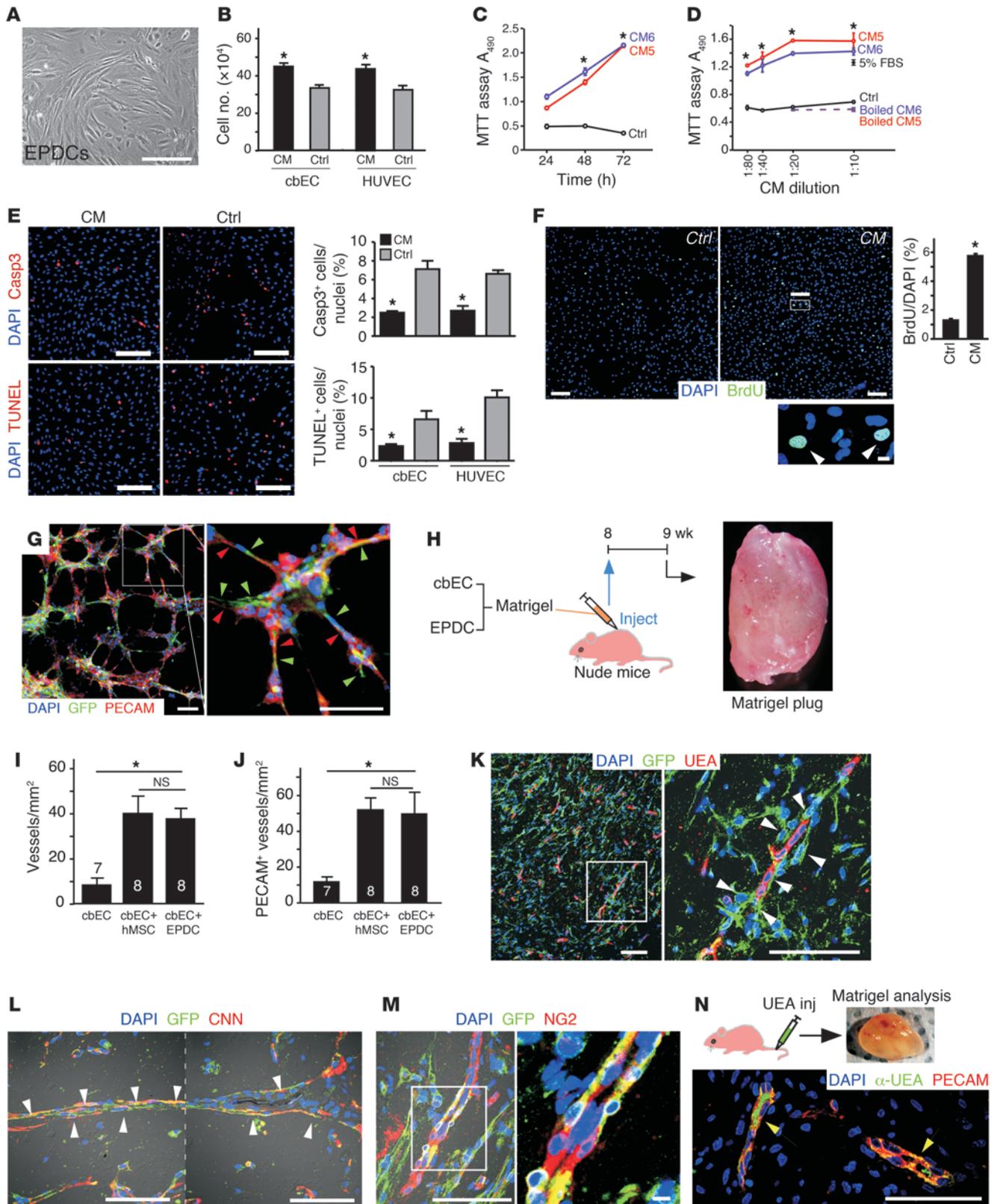
Figure 4

Paracrine effect of adult EPDCs. (**A**) Morphology of P5 EPDCs. (**B**) EPDC-CM (1:10 dilution) increased EC number compared with control medium. Cell number was determined by direct counting. *n* = 4. (**C** and **D**) EPDC-CM stimulated EC growth, measured by MTT assay. cbECs were cultured with CM at the indicated dilution and duration. (**E**) Quantification of ECs stained with cleaved caspase 3 (Casp3) or TUNEL. *n* = 3. (**F**) BrdU assay of cbECs cultured with EPDC-CM or control medium. *n* = 4. (**G**) EPDCs coculture with cbECs on Matrigel-stimulated tubule formation. EPDCs (green arrowheads) incorporated the vessel-like tubular network formed by cbECs (red arrowheads). (**H**) EPDC-stimulated angiogenesis in vivo in Matrigel plug assay. Matrigel and cbECs were injected into nude mice alone or in combination with EPDCs or human MSCs (hMSC; positive control). (**I** and **J**) Density of blood-filled and PECAM⁺ vessels in plugs. *n* = 7–8. (**K**–**M**) Immunostaining of Matrigel plug sections showed that EPDCs (GFP⁺, white arrowheads) were located adjacent to human ECs (UEA⁺) (**M**) and expressed smooth muscle (CNN) and pericyte (NG2) markers (**L** and **M**). (**N**) Tail vein injection of UEA-labeled ECs within the Matrigel plug (yellow arrows) demonstrated functional connection of cbEC-derived plug vessels with systemic vessels. Scale bars: 200 μm; 10 μm (**F**, bottom, and **M**, right). *n* is shown for each group in **I** and **J**. *$P < 0.05$ versus respective control.

MI creates a hypoxic environment, which can regulate angiogenic gene transcription and translation (15). To determine whether hypoxia influences EPDC production of angiogenic factors, we obtained CM from post-MI EPDCs cultured in normoxia or hypoxia. Hypoxia upregulated VEGFA levels, as determined by quantitative ELISA (Figure 5D). We also detected FGF2 upregulation under hypoxic conditions, and similar observations were made using an epicardial cell line (ref. 16 and data not shown). These data suggest that hypoxia may dynamically upregulate secretion of proangiogenic factors from the epicardial layer after MI.

Collectively, our data support a role for EPDCs as a source of angiogenic factors in the infarcted heart. This effect is partially mediated by VEGFA and FGF2, secretion of which increases under hypoxic conditions.

EPDC-CM reduced infarct size and improved heart function. To test the hypothesis that EPDC-secreted factors have a beneficial effect on the myocardial response to MI, we injected EPDC-CM or unconditioned media into the ischemic border zone immediately after inducing experimental MI. At 5–6 days after MI, triphenyltetrazolium chloride (TTC) staining showed that CM significantly reduced infarct size compared with control ($P < 0.05$; Figure 6A). Correspondingly, we observed increased vessel density in EPDC-CM–treated myocardium ($P < 0.05$; Figure 6B). To assess the effect of CM on heart function, we used both MRI and hemodynamic measurements 5–6 days after MI. MRI showed that LV ejection fraction, a measure of systolic heart function, was significantly increased in CM compared with control (Figure 6C). In Langendorff-perfused, isovolumetric heart preparations, systolic function improved with CM treatment, as measured by significant increases in peak and developed systolic pressure under baseline conditions and with dobutamine stress ($P < 0.05$; Figure 6, D–F). E_{max}, a load-independent measure of contractility, was also significantly improved by CM (Figure 6F). LV stiffness, which is inversely related to diastolic function, was reduced with CM injection ($P = 0.015$; Figure 6G), indicating that CM also beneficially affects diastolic function. Taken together, our data demonstrate that at an early time point, CM improves cardiac function of infarcted hearts both at baseline and upon increased workload.

Finally, we tested the effects of CM on cardiac function at a more distant time point. At 9 weeks after MI, EPDC-CM treatment at the time of left anterior descending coronary artery (LAD) ligation significantly reduced adverse cardiac remodeling, as shown by decreased LV systolic and diastolic volume in the CM-treated group (Supplemental Figure 14, A and B). There was a trend toward higher ejection fraction with CM treatment ($P = 0.076$; Supplemental Figure 14C). However, hemodynamic measurements in Langendorff-perfused hearts were not significantly different between groups (Supplemental Figure 14, D–G). Thus, CM treatment at the time of MI reduced cardiac remodeling, but did not significantly improve measures of cardiac function.

Discussion

Better understanding of the endogenous myocardial injury response will illuminate mechanisms that can be therapeutically modulated to minimize myocardial loss after MI and to amplify the limited regenerative capacity of mammalian myocardium. Using 2 independent genetic lineage-tracing methods, we investigated the cellular and paracrine contributions of epicardium to the MI injury response (Supplemental Figure 13). Whereas epicardium was quiescent in the normal heart, MI reactivated a fetal-like state, including proliferation, embryonic gene expression, and EMT. After MI, the epicardial layer expanded substantially, and a large fraction of cells expressed the *Wt1* epicardial marker. The increased number of WT1⁺ cells was likely due to both proliferation of these cells and reactivation of WT1 expression in previously nonexpressing cells. However, the injury-activated adult EPDCs appeared to incompletely recapitulate the properties of fetal EPDCs. Unlike fetal EPDCs (which migrate into myocardium and differentiate into cardiomyocytes, smooth muscle cells, interstitial cells, and ECs), post-MI adult EPDCs largely remain on the surface of the heart. Furthermore, as determined by both *Wt1^CreERT2* and Ad:Msln-Cre labeling approaches, adult EPDCs no longer differentiate into cardiomyocytes or ECs. A prior lineage-tracing study based on lentiviral labeling of epicardial cells using CMV-GFP suggested that epicardial cells differentiate into both ECs and cardiomyocytes after MI (11). The discrepancy with our results indicates that either the lentiviral labeling approach marked an epicardial population distinct from that labeled by *Wt1^CreERT2*, or the lentiviral label was not precisely confined to the epicardium. The molecular mechanisms underlying diminished mobilization and plasticity of adult epicardium are unknown, but may partially contribute to the reduced regenerative ability of adult heart. Enabling adult epicardium to more fully recapitulate its fetal properties may enhance the adult heart's regenerative capacity.

Another important function of fetal epicardium is to regulate myocardial growth and coronary development through secretion of paracrine factors. Therefore, we investigated whether EPDCs affect the adult myocardial injury response through paracrine mechanisms. Our data indicated that EPDC paracrine factors promote enhanced survival and growth of coronary vessels after MI. During development, coronary vessels form immediately under epicardium, stimulated by epicardial secretion of proangiogenic factors including VEGFA, FGF9/16/20, Sonic hedgehog, and WNT9b (17–21). MI reactivates fetal epicardial properties, and post-MI EPDCs secreted factors with potent proangiogenic activity in vitro and in vivo. We identified a number of factors with substantial enrichment in epicardium, including VEGFA and FGF2, and showed that these 2 factors contributed to angiogenic activity of EPDC-CM. However, other factors and their synergy are also important, as blocking both VEGFA and FGF2 only
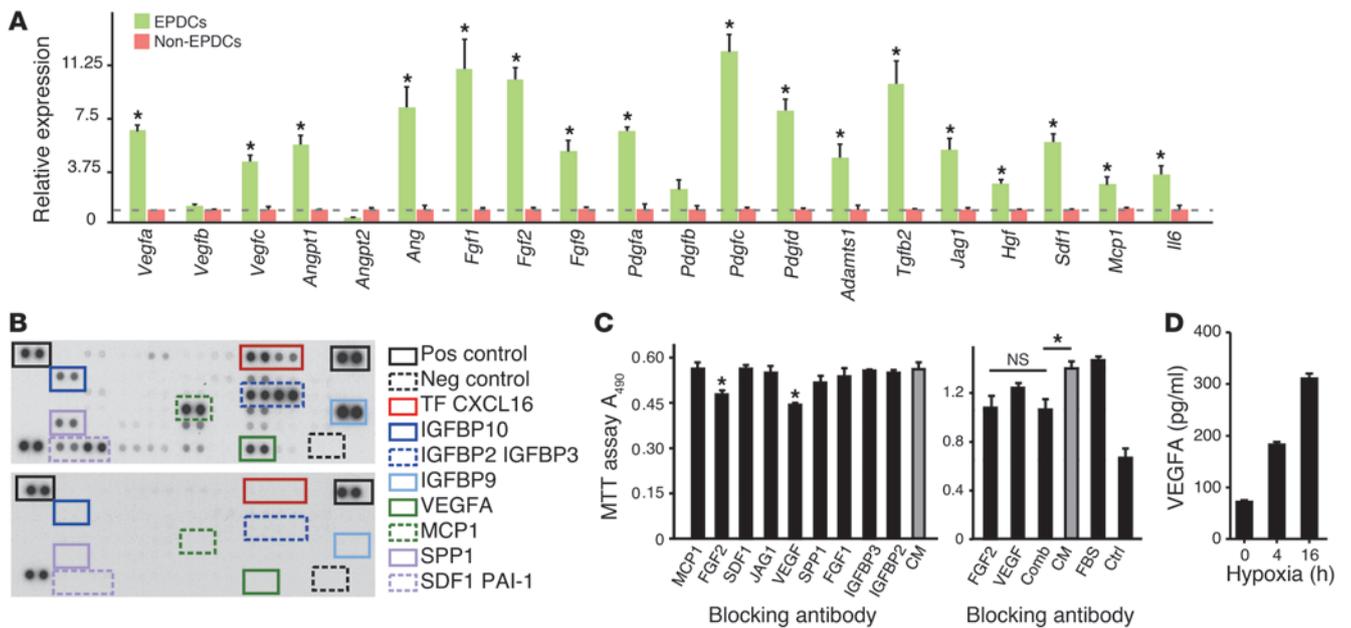
Figure 5
EPDC secretion of proangiogenic factors. (**A**) Enriched expression of angiogenic factors in EPDCs 1 week after MI. Expression was measured by qRT-PCR. $n = 3–6$. (**B**) Representative result of angiogenesis antibody array probed with EPDC-CM. Boxes indicate several key angiogenesis factors secreted by EPDCs. (**C**) Neutralizing antibodies showed that VEGFA and FGF2 contribute to the growth-promoting properties of CM. Control indicates no antibody addition. Growth was measured by MTT assay. FGF2 and VEGFA blockade reduced the growth-stimulating activity of CM by about 50%, but combined blockade (Comb) did not further inhibit CM activity. (**D**) Hypoxia-stimulated EPDC secretion of VEGFA. VEGFA in media was measured by ELISA and antibody array (not shown). Results are representative of 2 repeats. *$P < 0.05$.

partially inhibited CM activity. Candidates include PDGF-CC (22), placental growth factor (PLGF; ref. 23), and PDGF-BB (24).

Our present work showed that EPDCs secrete paracrine factors that participate in the myocardial injury response. Remarkably, injection of EPDC-CM reduced infarct size and improved heart function at 1 week after MI. At 9 weeks after MI, the single CM treatment reduced adverse cardiac remodeling, but the improvement in cardiac contractile performance was not sustained. MI reactivates fetal-like epicardial properties and stimulates dramatic expansion of EPDCs that amplifies epicardial paracrine signaling. The beneficial effect of EPDC-CM injected at the time of MI may result in part from immediate availability of protective EPDC factors that normally would not approach maximal availability for several days. Consistent with our findings of beneficial EPDC-CM activity, myocardial injection of human EPDCs in a murine MI model improved ventricular function, vascularization, wall thickness, and survival to 6 weeks, although there was no significant EPDC engraftment at this time point (25). More prolonged availability of EPDC-secreted factors with EPDC injection may account for the sustained functional benefit seen in this model. Thus, effective translation of the beneficial activity of EPDC-CM will require defining its active components and developing improved methods for sustained delivery.

We showed that one beneficial effect of EPDC-CM is to protect and augment coronary vasculature, which may promote survival of tenuous myocardium in the peri-infarct zone. Additional mechanisms, such as protection of cardiomyocytes from apoptosis or stimulation of cardiomyocyte progenitor expansion and differentiation, may also contribute to the protective effects of EPDC-CM. Further beneficial effects of EPDC-CM may arise from recruitment of other cell types. Consistent with marked upregulation of *Mcp1*

and *Sdf1* in infarcted EPDCs, we observed substantial infiltration of monocytes into the thickened post-MI epicardium (B. Zhou and W.T. Pu, unpublished observations), where they may contribute to the angiogenic response after MI (26). Further studies will be required to dissect the likely pleiotropic effects of EPDC-CM.

In this study, we described and validated approaches to genetically label and track EPDCs in the adult heart. This allowed us to assess, for the first time to our knowledge, the fate of adult epicardial cells after myocardial injury. We also developed methods to isolate adult post-MI EPDCs and to amplify them in culture. Amplification in culture was essential to make investigation of EPDC functional properties experimentally feasible. Expression of most EPDC gene and surface markers that we measured did not change substantially through 5 passages in culture, but we cannot exclude the possibility that culture-induced changes in EPDC-secreted factors contribute to the observed activity of EPDC-CM. Identification of the factors responsible for EPDC-CM activity will be needed to fully address this point and to facilitate studies of the long-term benefits of EPDC paracrine factors after MI.

In summary, our data suggest that post-MI EPDCs condition a subepicardial niche and that one action of EPDC-secreted factors is to promote survival and growth of blood vessels. Studies in zebrafish heart regeneration support the concept of a subepicardial niche. As we saw in mice, zebrafish heart apex amputation stimulated organ-wide fetal reactivation of epicardium that contributed to vascular development of the regenerate (2). Moreover, apex amputation stimulated proliferation of subepicardial cardiomyocytes, which subsequently replaced the amputated cardiomyocytes (27, 28). Our data suggest that a mammalian subepicardial niche, conditioned by factors secreted from the expanded EPDC layer, supports
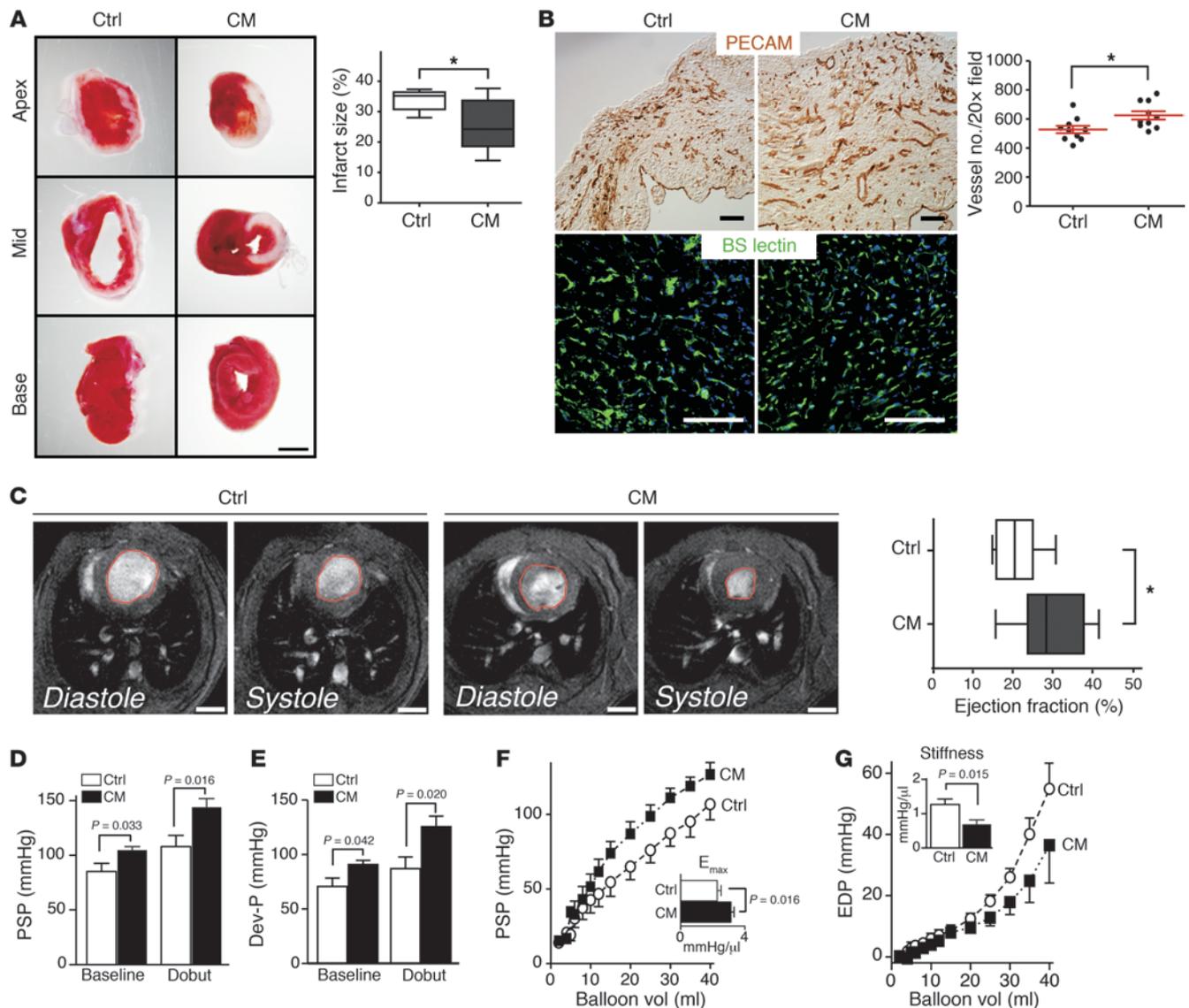
Figure 6
EPDC-CM reduced infarct size and improved heart function. (**A**) EPDC-CM reduced infarct size at 1 week. 1-mm short axis slices of heart were stained with TTC, and the infarct size (white color) was measured. $n = 6$. (**B**) Vessel density in peri-infarct area 1 week after MI. Representative images of PECAM and BS-1 lectin stained sections are shown. BS-1 quantitation showed increased vessel density in the CM-treated group. $n = 10$. (**C**) Cine-MR images obtained 5–6 days after MI. Red line indicates the chamber area. Ejection fraction, calculated from 5 stacked slices, was significantly higher with CM versus control treatment. $n = 8$. (**D**–**G**) LV systolic and diastolic function improved with CM treatment. Peak systolic pressure (PSP; **D** and **F**), developed systolic pressure (Dev-P; **E**), and E_{max} (**F**, inset), measures of systolic function, were higher with CM at baseline and with dobutamine stress. LV stiffness (**G**, inset), reciprocally related to diastolic function, was improved with CM. EDP, end-diastolic pressure. $n = 9$ (control); 6 (EPDC-CM). Scale bars: 2 mm (**A**); 100 μm (**B**); 2.5 mm (**C**). In **A** and **C**, lines within boxes denote median, boxes denote interquartile range, and whiskers denote range. *$P < 0.05$.

blood vessel survival and growth. We hypothesize this niche also favors survival, growth, and differentiation of cardiomyocytes and their progenitors; future experiments will test this hypothesis. The EPDC-conditioned subepicardial niche provides what we believe to be a new paradigm to study the myocardial injury response in mammals, and augmentation of the subepicardial niche may represent a novel therapeutic strategy to improve outcome from MI.

Methods

Further information can be found in Supplemental Methods.

All experiments with mice were performed according to protocols approved by the Institutional Animal Care and Use Committees of Children's Hospital Boston or Beth Israel Deaconess Medical Center. *Wt1*$^{GFPCre/+}$, *Wt1*$^{CreERT2/+}$, *Rosa26*$^{fsLz/+}$, *iTNT-Cre*, and *Rosa26*$^{mTmG/+}$ mice were described previously (4, 29–32). We administered tam (1 mg/10 g body weight) by gavage to pregnant mice at E10.5 to induce Cre. For adult mice, 4 mg tam (Sigma-Aldrich) was administered by gavage to 6- to 9-week-old mice twice weekly for 2–3 weeks.

MI was induced by ligation of LAD through a thoracotomy, as described previously (33). Sham operation included opening of the pericardium, but not ligation of the coronary artery. Where indicated, concentrated CM or

unconditioned media were injected into the infarct border zone at the time of LAD ligation. Measurement of heart function by MRI was performed on anesthetized mice using gated Flash-CINE sequences. Langendorff perfusion was performed as described previously (34).

EPDCs were isolated from apical regions of hearts by collagenase digestion to obtain single-cell suspensions, followed by FACS sorting as described previously (35). After recovery, cells were amplified in MSC growth media (Lonza) with 10% FBS. For preparation of CM, cells were switched to EBM2 (Lonza) without serum for 24 hours. Media was then collected and concentrated 30-fold.

EC growth was measured by MTT assay (Promega) and direct counting. EC apoptosis was measured by TUNEL and cleaved caspase-3 assays (Roche; Cell Signaling Technology). Tubule formation, Matrigel plug, and corneal angiogenesis assays were performed as described previously (36–38).

Immunohistochemistry and spectral emission analyses were performed as described previously (39, 40), using antibodies listed in Supplemental Table 1. Gene expression was analyzed by qRT-PCR using the $\Delta\Delta C_t$ method and primers listed in Supplemental Table 2.

Statistical analysis was performed using 2-tailed Student's t test. A P value less than 0.05 was considered significant. Values are reported as mean ± SEM.

1. Hsieh PC, et al. Evidence from a genetic fate-mapping study that stem cells refresh adult mammalian cardiomyocytes after injury. *Nat Med*. 2007; 13(8):970–974.
2. Lepilina A, et al. A dynamic epicardial injury response supports progenitor cell activity during zebrafish heart regeneration. *Cell*. 2006;127(3):607–619.
3. Cai CL, et al. A myocardial lineage derives from Tbx18 epicardial cells. *Nature*. 2008;454(7200):104–108.
4. Zhou B, et al. Epicardial progenitors contribute to the cardiomyocyte lineage in the developing heart. *Nature*. 2008;454(7200):109–113.
5. Wilm B, Ipenberg A, Hastie ND, Burch JB, Bader DM. The serosal mesothelium is a major source of smooth muscle cells of the gut vasculature. *Development*. 2005;132(23):5317–5328.
6. Dettman RW, Denetclaw WJ, Ordahl CP, Bristow J. Common epicardial origin of coronary vascular smooth muscle, perivascular fibroblasts, and intermyocardial fibroblasts in the avian heart. *Dev Biol*. 1998;193(2):169–181.
7. Gittenberger-de Groot AC, Vrancken Peeters MP, Mentink MM, Gourdie RG, Poelmann RE. Epicardium-derived cells contribute a novel population to the myocardial wall and the atrioventricular cushions. *Circ Res*. 1998;82(10):1043–1052.
8. Robinson C, et al. A novel SV40 TAg transgenic model of asbestos-induced mesothelioma: malignant transformation is dose dependent. *Cancer Res*. 2006; 66(22):10786–10794.
9. Urwin D, Lake RA. Structure of the Mesothelin/MPF gene and characterization of its promoter. *Mol Cell Biol Res Commun*. 2000;3(1):26–32.
10. Wagner KD, et al. The Wilms' tumor suppressor Wt1 is expressed in the coronary vasculature after myocardial infarction. *FASEB J*. 2002;16(9):1117–1119.
11. Limana F, et al. Identification of myocardial and vascular precursor cells in human and mouse epicardium. *Circ Res*. 2007;101(12):1255–1265.
12. Red-Horse K, Ueno H, Weissman IL, Krasnow MA. Coronary arteries form by developmental reprogramming of venous cells. *Nature*. 2010; 464(7288):549–553.
13. Lavine KJ, Ornitz DM. Fibroblast growth factors and Hedgehogs: at the heart of the epicardial signaling center. *Trends Genet*. 2008;24(1):33–40.
14. Arminan A, et al. Mesenchymal stem cells provide better results than hematopoietic precursors for the treatment of myocardial infarction. *J Am Coll Cardiol*. 2010;55(20):2244–2253.

15. Rey S, Semenza GL. Hypoxia-inducible factor-1-dependent mechanisms of vascularization and vascular remodelling. *Cardiovasc Res*. 2010;86(2):236–242.
16. Wada AM, Smith TK, Osler ME, Reese DE, Bader DM. Epicardial/Mesothelial cell line retains vasculogenic potential of embryonic epicardium. *Circ Res*. 2003;92(5):525–531.
17. Wu H, Lee SH, Gao J, Liu X, Iruela-Arispe ML. Inactivation of erythropoietin leads to defects in cardiac morphogenesis. *Development*. 1999; 126(16):3597–3605.
18. Lavine KJ, et al. Fibroblast growth factor signals regulate a wave of Hedgehog activation that is essential for coronary vascular development. *Genes Dev*. 2006;20(12):1651–1666.
19. Lavine KJ, et al. Endocardial and epicardial derived FGF signals regulate myocardial proliferation and differentiation in vivo. *Dev Cell*. 2005;8(1):85–95.
20. Merki E, et al. Epicardial retinoid X receptor alpha is required for myocardial growth and coronary artery formation. *Proc Natl Acad Sci U S A*. 2005; 102(51):18455–18460.
21. Zamora M, Manner J, Ruiz-Lozano P. Epicardium-derived progenitor cells require beta-catenin for coronary artery formation. *Proc Natl Acad Sci U S A*. 2007; 104(46):18109–18114.
22. Li X, et al. Revascularization of ischemic tissues by PDGF-CC via effects on endothelial cells and their progenitors. *J Clin Invest*. 2005;115(1):118–127.
23. Carmeliet P, et al. Synergism between vascular endothelial growth factor and placental growth factor contributes to angiogenesis and plasma extravasation in pathological conditions. *Nat Med*. 2001; 7(5):575–583.
24. Cao R, et al. Angiogenic synergism, vascular stability and improvement of hind-limb ischemia by a combination of PDGF-BB and FGF-2. *Nat Med*. 2003; 9(5):604–613.
25. Winter EM, et al. Preservation of left ventricular function and attenuation of remodeling after transplantation of human epicardium-derived cells into the infarcted mouse heart. *Circulation*. 2007; 116(8):917–927.
26. Iba O, et al. Angiogenesis by implantation of peripheral blood mononuclear cells and platelets into ischemic limbs. *Circulation*. 2002;106(15):2019.
27. Kikuchi K, et al. Primary contribution to zebrafish heart regeneration by gata4(+) cardiomyocytes. *Nature*. 2010;464(7288):601–605.
28. Jopling C, Sleep E, Raya M, Marti M, Raya A, Bel-

monte JC. Zebrafish heart regeneration occurs by cardiomyocyte dedifferentiation and proliferation. *Nature*. 2010;464(7288):606–609.
29. Muzumdar MD, Tasic B, Miyamichi K, Li L, Luo L. A global double-fluorescent Cre reporter mouse. *Genesis*. 2007;45(9):593–605.
30. Jiao K, et al. An essential role of Bmp4 in the atrioventricular septation of the mouse heart. *Genes Dev*. 2003;17(19):2362–2367.
31. Soriano P. Generalized lacZ expression with the ROSA26 Cre reporter strain. *Nat Genet*. 1999; 21(1):70–71.
32. Wu B, et al. Inducible cardiomyocyte-specific gene disruption directed by the rat Tnnt2 promoter in the mouse. *Genesis*. 2010;48(1):63–72.
33. Tarnavski O, McMullen JR, Schinke M, Nie Q, Kong S, Izumo S. Mouse cardiac surgery: comprehensive techniques for the generation of mouse models of human diseases and their application for genomic studies. *Physiol Genomics*. 2004;16(3):349–360.
34. He H, Javadpour MM, Latif F, Tardiff JC, Ingwall JS. R-92L and R-92W mutations in cardiac troponin T lead to distinct energetic phenotypes in intact mouse hearts. *Biophys J*. 2007;93(5):1834–1844.
35. Zhou B, von Gise A, Ma Q, Hu YW, Pu WT. Genetic fate mapping demonstrates contribution of epicardium-derived cells to the annulus fibrosis of the mammalian heart. *Dev Biol*. 2010;338(2):251–261.
36. Zhou B, et al. Fog2 is critical for cardiac function and maintenance of coronary vasculature in the adult mouse heart. *J Clin Invest*. 2009;119(6):1462–1476.
37. Melero-Martin JM, et al. Engineering robust and functional vascular networks in vivo with human adult and cord blood-derived progenitor cells. *Circ Res*. 2008;103(2):194–202.
38. Fernandez CA, Butterfield C, Jackson G, Moses MA. Structural and functional uncoupling of the enzymatic and angiogenic inhibitory activities of tissue inhibitor of metalloproteinase-2 (TIMP-2): loop 6 is a novel angiogenesis inhibitor. *J Biol Chem*. 2003; 278(42):40989–40995.
39. Zhou B, et al. G-CSF-mobilized peripheral blood mononuclear cells from diabetic patients augment neovascularization in ischemic limbs but with impaired capability. *J Thromb Haemost*. 2006; 4(5):993–1002.
40. D'Alessandro DA, et al. Progenitor cells from the explanted heart generate immunocompatible myocardium within the transplanted donor heart. *Circ Res*. 2009;105(11):1128–1140.